Considerations for surface reconstruction stability prediction on GaAs(001)

John C. Thomas, Anton Van der Ven, and Joanna Mirecki Millunchick*
Department of Materials Science and Engineering, University of Michigan, Ann Arbor, Michigan 48109, USA

Normand A. Modine
Center for Integrated Nanotechnologies, Sandia National Laboratories, Albuquerque, New Mexico 87185, USA.
(Received 21 April 2012; revised manuscript received 6 January 2013; published 25 February 2013)

We present a theoretical analysis of the finite-temperature equilibrium surface reconstruction stability of GaAs(001) from first principles, encompassing the As-rich regime relevant to low-temperature grown GaAs. Experimental evidence points to the thermodynamic stability of a (4×3) reconstruction in this regime, but density functional theory (DFT) calculations predict all (4×3) reconstructions to be metastable relative to the $\beta 2(2 \times 4)$ and $c(4 \times 4)$ reconstructions. We employ statistical mechanical simulations, parameterized by DFT to study the combined effects of configurational disorder and vibrational excitations on surface phase stability. The calculated finite-temperature surface free energies of the various reconstructions indicate that, if a small constant energy shift is used to enforce stability of the lowest-energy (4×3), the resultant phase diagram is consistent with experiment with the $c(4 \times 4)$ overwhelming (4×3) at high temperatures. This behavior is due to competition between configurational entropy, which favors $c(4 \times 4)$, and vibrational entropy, which favors (4×3).

DOI: 10.1103/PhysRevB.87.075320 PACS number(s): 68.35.Md, 68.35.B−, 68.35.Rh, 68.47.Fg

The broad importance of III-V compound semiconductors for device applications is due to their wide variety of realizable tunable alloys. However, because useful III-V alloys and heterostructures require precisely controlled layer-by-layer synthesis, their resultant properties and quality are largely limited by our understanding of structure and ordering phenomena at the crystalline growth surface. The structure and composition of the surface play an important role in the injection of point defects and antisites, particularly at low temperatures. Increasingly, these surface-induced defects are exploited for their beneficial consequences as in low-temperature-grown (LTG) GaAs, which is an important material for terahertz (THz) emitters and detectors.[1] LTG GaAs is typically grown in the [001] orientation at temperatures below 300 °C and under As-rich conditions.[2,3] In this regime, excess surface As becomes kinetically trapped in the growing film, incorporating at up to 1 at. % above bulk stoichiometry in the form of both antisite defects and metallic As precipitates.[2,4] The high charge mobility and very low carrier lifetime in defected LTG GaAs make it particularly well suited for THz-range heterodyne photomixers.[5,6] The low-temperature growth regime is also used to enhance incorporation in low-solubility alloy systems, such as $Ga_{1-x}Bi_xAs$ (Ref. 7) and the ferroelectric semiconductor $Ga_{1-x}Mn_xAs$ (Ref. 8).

Significant theoretical study of GaAs(001) has previously identified only two stable As-rich surface reconstructions, relative to bulk stoichiometry: the $c(4 \times 4)$ and $\beta 2(2 \times 4)$, illustrated in Figs. 1(a) and 1(b), respectively.[9–11] Experimental observations, however, indicate the existence of a stable "×3" surface reconstruction on GaAs(001) with an As coverage intermediate to that of the $\beta 2(2 \times 4)$ and $c(4 \times 4)$.[12–15] Scanning tunneling microscopy experiments strongly suggest that the GaAs ×3 surface actually consists of a (4×3) reconstruction.[14] Any complete description of GaAs(001) surface stability must account for this (4×3) reconstruction.

This paper presents our rigorous and comprehensive theoretical analysis of surface reconstruction stability on GaAs(001). We identify the low-energy As-rich GaAs(001) reconstruction prototypes and calculate their finite-temperature surface free energies from first principles, taking into account the combined effects of configurational disorder and vibrational excitations. By considering small relative shifts to the reconstruction surface free energies calculated from first principles, we reproduce the experimentally observed sequence of reconstruction stability with respect to temperature and surface composition. By relating the surface free energies to the finite-temperature partial pressure of As_4, we obtain a GaAs(001) surface phase diagram that is easily relatable to experimental results with which we find good agreement. By elucidating the link between thermal disorder and surface reconstruction stability, our results provide crucial insight about the role of thermal excitation when targeting desirable growth regimes.

Traditionally, surface reconstruction stability has been determined by comparing energies obtained from electronic structure calculations for a collection of reconstruction hypotheses. The reconstruction hypotheses are conjectured *a posteriori* based on limited empirical evidence. Consequently, constructing a hypothesis and verifying its stability are complicated by a number of factors. On a multicomponent surface, a well-specified surface reconstruction is composed of a reconstruction prototype, which defines the bonding topology of surface atoms, and a species configuration that decorates it; if a prototype specifies an arrangement of dimers on the surface, each possible configuration of that prototype specifies whether each dimer is a homodimer, composed of like species, or a heterodimer, composed of unlike species. Energy differences between reconstructions are calculated from density functional theory (DFT), which reliably predicts many ground-state properties of III-V compounds but provides no direct information about thermally excited behavior. Thermal effects, including lattice vibrations and fluctuations in species configuration, contribute an entropic component to the surface free energy that may alter reconstruction

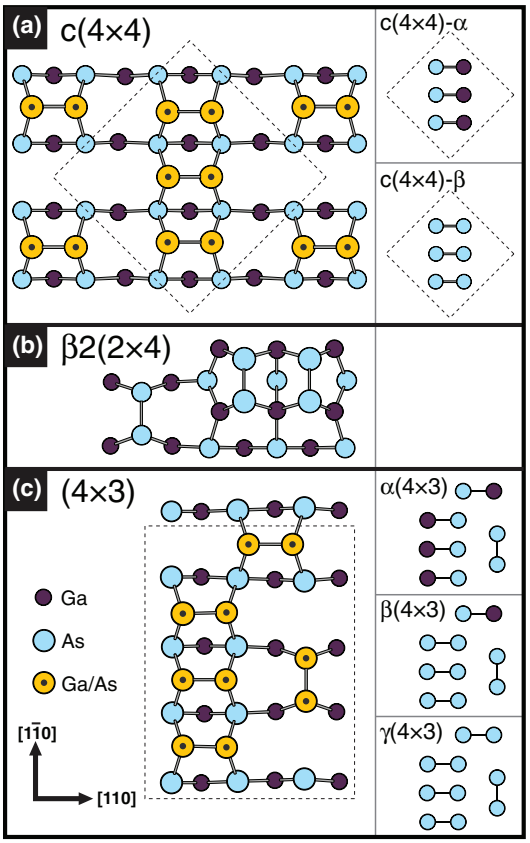

FIG. 1. (Color online) The low-energy As-rich reconstruction prototypes of GaAs(001). In (a) and (c), gold circles with black dots indicate variable sites, which can be either Ga or As. Inset images illustrate the most stable Ga/As species configurations of these sites.

stability. Consequently, 0-K surface energies, calculated from DFT, are an insufficient predictor of reconstruction stability. At typical synthesis temperatures ($k_BT \sim 50$–80 meV), a sufficient entropy difference between surface reconstructions can overwhelm the difference in their 0-K surface energies, resulting in *entropic* stabilization of one reconstruction relative to another.

Recent advances have resulted in a catalog of all plausible III-V surface reconstructions, enabling an exhaustive search for a low-energy (4×3) reconstruction on GaAs(001).[11] Among the 124 conceivable (4×3) reconstruction prototypes that are charge balanced, DFT calculations indicate that the prototype that is depicted in Fig. 1(c) has the lowest surface energy. Two species configurations of this prototype, the $\alpha(4 \times 3)$ and $\beta(4 \times 3)$, have previously been predicted to be stable on the GaSb(001) and AlSb(001) surfaces.[16] These are illustrated in the Fig. 1(c) inset. However, DFT predicts all species configurations of this (4×3) to be *metastable* on GaAs(001) relative to either $\beta 2(2 \times 4)$ or at least one species configuration of the $c(4 \times 4)$ prototype. The difference in surface free energy between the (4×3) and the $c(4 \times 4)$ prototypes is very small, though—approximately 7 meV/$A_{(1\times1)}$ over a sizable range of chemical potential, where $A_{(1\times1)}$ is the area of the surface primitive cell. Our calculations for the 123 other charge-balanced (4×3) prototypes show them to have much higher surface energies with respect to the $c(4 \times 4)$ (see Supplemental Material).[17] Consequently, the only (4×3) prototype that merits consideration is the one depicted in Fig. 1(c).

The multicomponent surface is an open system at fixed temperatures such that the surface free energy $\gamma(T, \mu_{As})$ is minimized at equilibrium for fixed temperature T and As chemical potential μ_{As}.[17] γ includes contributions from electronic structure (i.e., the 0-K surface enthalpy), configurational excitations, and lattice vibrations. Electronic structure calculations were performed using a surface/slab geometry within the DFT local-density approximation (LDA) as implemented in the Vienna *ab initio* simulation package (VASP).[18] Procedures and parameters are well established for DFT calculations of III-V surface systems.[17]

In GaAs(001), configurational entropy arises from the many possible arrangements of Ga and As over the tricoordinate surface sites of the (4×3) and $c(4 \times 4)$ prototypes. These undercoordinated sites have three sp^3-hybridized interatomic bonds; the fourth sp^3 orbital is a "dangling bond." As suggested by the electron counting heuristic,[19] the dangling bond allows Ga and As to substitute at these sites without affecting surface charge balance. Consequently, thermal excitations can sample many different configurations of Ga and As on the lattice of tricoordinate sites. Figures 1(a) and 1(c) indicate the sites that can undergo low-energy species substitution in the (4×3) and $c(4 \times 4)$ prototypes. Energies of many Ga/As configurations were calculated for each prototype and, via the cluster expansion (CE) formalism,[20,21] were used to construct an effective Hamiltonian for arbitrary configurations of the prototype. The (4×3) and $c(4 \times 4)$ reconstructions were considered separately, resulting in two prototype-specific cluster expansions.[17] The CE formalism and fitting procedure for surface systems have been discussed in detail elsewhere.[22]

Surface vibrational free energies were evaluated using an Einstein model, which has been used to study other covalently bonded surface systems.[23] Vibrational frequencies of each site were calculated using the finite-difference implementation in VASP by diagonalizing the single-site Hessian tensor. The calculated vibrational frequencies were nearly independent of surface species configuration, allowing us to express the vibrational free energy of each substitution site in terms of only the on-site nearest-neighbor species occupant. Calculated vibrational free energies in lower layers are independent of the Ga/As surface configuration to within ~1 meV/$A_{(1\times1)}$ at synthesis temperatures. The total effective Hamiltonian efficiently predicts combined configurational energy and vibrational free energy for arbitrary configurations of a prototype, making it well suited for use in Metropolis Monte Carlo (MC) simulations.

Finite-temperature surface free energies were integrated from equilibrium MC simulations for both the As-rich (4×3) and the $c(4 \times 4)$ reconstruction prototypes.[17] DFT calculations indicate a large energy penalty for Ga/As substitution in the $\beta 2(2 \times 4)$ due to the consequent formation of high-energy Ga-Ga bonds, allowing us to neglect its configurational excitations, leaving only vibrational excitations. Thus, the surface free energy of the single $\beta 2(2 \times 4)$ configuration shown in Fig. 1(b) was used to bound the range of μ_{As} relevant to As-rich growth. The GaAs(001) surface phase diagram was constructed by minimizing the surface free energy over $\gamma_{\beta 2(2\times4)}$, $\gamma_{(4\times3)}$, and

$\gamma_{c(4\times4)}$ with respect to μ_{As} and T. First-order phase boundaries occur where minimal surface free energies cross.

The equilibrium conditions among bulk metallic As, bulk GaAs, and polyatomic As_m gas specify an expression for the normalized As_m partial pressure,

$$\tilde{p}_{As_m} = \frac{p^{(As_m)}}{p_0^{(As_m)}(T)} = \exp\left[m\frac{\mu_{As} - g_{As}^{(bulk)}}{k_B T}\right], \qquad (1)$$

where $p_0^{(As_m)}$ is the vapor pressure of As_m over bulk As and $g_{As}^{(bulk)}$ is the per-atom Gibbs free energy of bulk As. Therefore, we may visualize phase stability as a function of T and $\tilde{p}_{As_4}$; the use of As_2 only alters the slopes of phase boundaries in an Arrhenius representation. The natural upper limit of $\tilde{p}_{As_m}$ occurs at $\tilde{p}_{As_m} \geqslant 1$ where zinc-blende GaAs becomes thermodynamically unstable relative to bulk As.

Calculated free energies predict that the (4×3) is metastable relative to $c(4 \times 4)$ and $\beta2(2 \times 4)$ for all $\tilde{p}_{As_m}$ and T. However, the difference in surface energy that exists between the (4×3) and the $c(4 \times 4)$ is unusually small relative to other III-V surface stability problems. MC simulations yield a (4×3) surface free energy $\gamma_{(4\times3)}$ that lies only 6 meV/$A_{(1\times1)}$ above $\gamma_{c(4\times4)}$ at low temperatures near 400 K, despite experimental observation of a (4×3) at similar temperatures.[12,14] We also compared a subset of the lowest 0-K surface energies calculated in the LDA to equivalent calculations performed in the generalized gradient approximation (GGA) to DFT and found that the GGA predicts the $c(4 \times 4)$ to be slightly more stable relative to (4×3) on average than the LDA (by an additional 2 to 3 meV/$A_{(1\times1)}$).

Despite the disagreement between experiment and predictions of various approximations to DFT, examining the temperature dependence of the calculated surface free energies in the context of experimental observations provides compelling evidence that the (4×3) is, in fact, a stable low-temperature surface phase and that its appearance cannot simply be attributed to kinetic effects. In particular, the calculated free energies indicate that the $c(4 \times 4)$ becomes even more stable with increasing temperature due to its relatively large configurational entropy. This trend is robust and is due predominantly to differences in the areal density of low-energy substitution sites in the (4×3) versus the $c(4 \times 4)$ prototype. As such, we can surmise that, if the (4×3) is stable, it occurs only at low temperatures and that its observation is not due to kinetic trapping of a high-temperature surface. Cooling a $c(4 \times 4)$ surface from high temperatures would instead give rise to a (4×3) via a nucleation and growth mechanism with its accompanying interface and strain energy penalties. The fact that the (4×3) requires carefully controlled conditions and annealing of the surface in order to manifest experimentally suggests that there is a small but real thermodynamic driving force to overcome these nucleation barriers, meaning that $\gamma_{(4\times3)}$ must actually be less than $\gamma_{c(4\times4)}$ at low temperatures. Our exhaustive enumeration of the most likely (4×3) surface structures and analysis of their stability with DFT provides particularly compelling evidence that, if a (4×3) surface phase is stable on GaAs(001), it is described by the $h0(4 \times 3)$ prototype depicted in Fig. 1(c).[17]

We can explore plausible scenarios for phase stability by considering a range of scenarios in which DFT slightly overpredicts the 0-K surface energy of the (4×3) configurations by small amounts. Rigid negative shifts to the (4×3) surface free energy < 9.5 meV/$A_{(1\times1)}$ yield a thermodynamically stable (4×3) phase and a phase diagram topology very similar to that of the experimental phase diagram. Figure 2 shows the calculated GaAs(001) surface phase diagram using three different rigid shifts of the (4×3) DFT surface energies relative to $\beta2(2 \times 4)$ and $c(4 \times 4)$ (alternatively, considering rigid shifts to $\gamma_{c(4\times4)}$ yields nearly equivalent results). The solid (4×3) phase boundary in Fig. 2, obtained by shifting $\gamma_{(4\times3)}$ downward by 8.5-meV/$A_{(1\times1)}$, most closely resembles experimental results, but the stability of the (4×3) is very sensitive to small shifts in its surface free energy; alternate phase boundaries, obtained by shifting $\gamma_{(4\times3)}$ downward by 8.0 and 9.0 meV/$A_{(1\times1)}$, are also shown. Shifting $\gamma_{(4\times3)}$ by more than 9.5 meV/$A_{(1\times1)}$ qualitatively changes the phase diagram as the (4×3) overwhelms the region of $c(4 \times 4)$ stability bordering the $\beta2(2 \times 4)$. By comparing LDA and GGA surface energies, we can estimate that DFT calculations are only able to accurately resolve surface energy differences larger than approximately ± 9.7 meV/$A_{(1\times1)}$ on GaAs as determined from the variation in surface energies calculated using the two correlation-exchange functionals.[17]

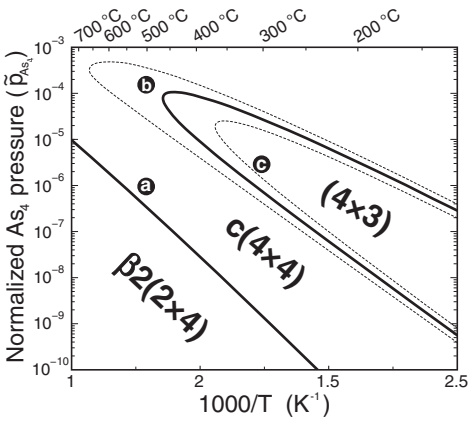

FIG. 2. Calculated GaAs(001) surface reconstruction phase diagram as a function of inverse temperature and normalized partial pressure. The (4×3) surface free energy has undergone a negative shift of 8.5 meV/$A_{(1\times1)}$ relative to that of the $c(4 \times 4)$. Alternate phase boundaries are shown for 8-meV/$A_{(1\times1)}$ and 9-meV/$A_{(1\times1)}$ negative shifts. Circles a–c indicate the thermodynamic parameters corresponding to MC snapshots in Fig. 3.

Although the choice of correlation-exchange functional is certainly the largest source of error in DFT, other approximations also reduce calculation accuracy, including plane-wave basis-set truncation, incompatibility of k-point meshes between different unit cells, and numerical discretization. Additionally, it should be noted that any combination of shifts to the surface free energies can be projected onto two independent qualitative changes to the phase diagram topology: shifting the position of the $\beta2(2 \times 4)$-$c(4 \times 4)$ boundary and shifting the position of the (4×3)-$c(4 \times 4)$ boundary. The $\beta2(2 \times 4)$-$c(4 \times 4)$ boundary is largely insensitive to small energy changes due to the relatively large stoichiometric difference between the $\beta2(2 \times 4)$ and the other two phases.

The phase diagram in Fig. 2 bears a strong resemblance to the comparable region of the experimental phase diagram determined using reflection high-energy electron diffraction (RHEED).[12] In particular, the solid (4×3) phase boundary in Fig. 2 is consistent with the $\times 3$ phases on the RHEED phase diagram, and the predicted (4×3)-$c(4 \times 4)$ transition temperature of 460 °C coincides with the maximum temperature at which $\times 3$ was observed. Also, both the experimental and the computed phase diagrams exhibit a range of As_4 isobars that pass, with increasing temperature, from (4×3) to $c(4 \times 4)$ and then to (2×4). Nevertheless, it is difficult to draw precise comparisons with experimental results. Observations of various $(n \times 3)$ reconstructions have been reported with $n \leqslant 4$, although these have been attributed to the effective diffraction pattern of a (4×3) reconstruction interrupted by long-range disorder.[24] Similarly, a combination of kinetic effects and lack of long-range order may account for the appearance of a (2×1) reconstruction along the $c(4 \times 4)$-$\beta 2(2 \times 4)$ phase boundary on the RHEED phase diagram reported by Däweritz and Hey.[12] The very small differences in calculated surface free energies among all three reconstruction prototypes in this region suggest a high likelihood of disorder, and/or hysteretic effects could occur. As a consequence, a reduction in apparent periodicity, as measured by RHEED, is not unexpected in this regime.

Because this study considers the combined effect of vibrational and configurational excitations on the finite-temperature surface reconstruction stability of a prototypical III-V material, our results elucidate the importance of thermal disorder in reconstruction stabilization on III-V surfaces. Our analysis indicates that configurational and vibrational excitations can have opposing effects. Calculation of each effect independently shows that vibrations enhance stability of the (4×3) prototype, particularly at low temperature, whereas configurational excitations favor stability of the $c(4 \times 4)$ reconstruction.[17] Vibrational effects favor the (4×3) due to its high density of undercoordinated surface sites, which have lower vibration frequencies than subsurface sites. The strong influence of configuration on $c(4 \times 4)$ stability is partly due to its ordering phenomena at low temperatures where the short-range order specific to the $c(4 \times 4)$-β occurs on the As-rich side of Fig. 2 and the short-range-order characteristic of the $c(4 \times 4)$-α occurs proximal to the $\beta 2(2 \times 4)$ phase boundary as shown in Fig. 3(a). At low temperatures, the transition between these two regimes of short-range order on the $c(4 \times 4)$ occurs abruptly (although it is not a formal phase transition) in the region where we propose the (4×3) to be stable. At higher temperatures, the regions of $c(4 \times 4)$ short-range order are separated by a region of configurational disorder as demonstrated by Fig. 3(b). Where the (4×3) occurs on the calculated phase diagram, it predominantly exhibits $\beta(4 \times 3)$ order as shown in Fig. 3(c).

These findings suggest strategies to control surface disorder and, thereby, to influence defect incorporation during growth. For example, a $c(4 \times 4)$ surface, obtained by decreasing As overpressure along an isotherm originating from a (4×3) surface, will result in a relatively well-ordered $c(4 \times 4)$-α surface configuration. Conversely, approaching the $c(4 \times 4)$ by increasing temperature along an isobar that originates from a (4×3) surface should produce a disordered $c(4 \times 4)$ surface.

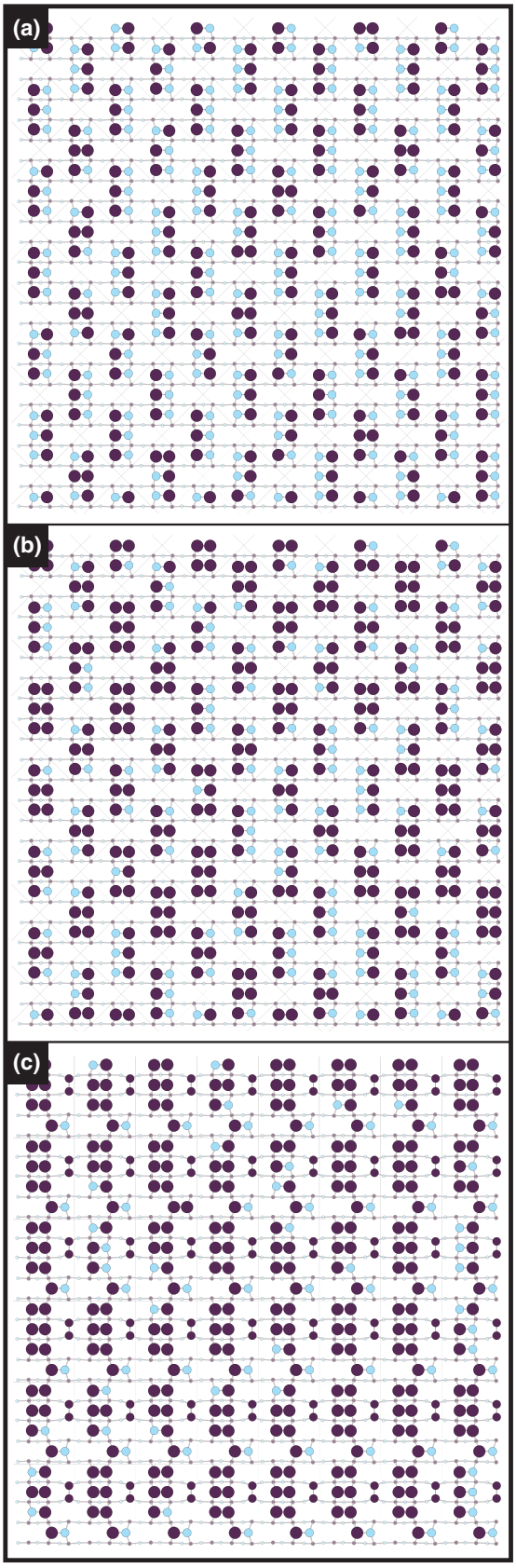

FIG. 3. (Color online) Instantaneous snapshots of the MC simulation cell at the three thermodynamic points indicated in Fig. 2. The illustrated regimes are (a) $c(4 \times 4)$-α short-range order, (b) $c(4 \times 4)$ disorder, and (c) $\beta(4 \times 3)$ short-range order.

To summarize, we have proposed a surface phase diagram for As-rich GaAs(001) based on rigorous first-principles calculations. Our phase diagram is informed by experimental observations in regions of thermodynamic phase space where DFT cannot reliably resolve the very small energy differences that distinguish stable reconstructions from metastable reconstructions. By first screening all possible charge-balanced (4×3) reconstruction prototypes, we identified only one prototype that could be stabilized within the energy range of DFT accuracy. Finite-temperature surface free energies of the stable As-terminated surface phases, which rigorously accounted for vibrational and configurational excitations, demonstrated that our proposed (4×3) prototype can be stabilized only at low temperatures, whereas the $c(4 \times 4)$ prototype is entropically stabilized at elevated temperatures, in good agreement with the experimental literature. These results resolve the characterization problem of the GaAs(001) (4×3) surface phase. Furthermore, they provide a solid thermodynamic foundation from which to understand and to manipulate incorporation of point defects during low-temperature growth.

We gratefully acknowledge support from DOE/BES (Grant No. ER 46172). Sandia is a multiprogram laboratory operated by Sandia Corporation, a Lockheed Martin Company, for the US Department of Energy under Contract No. DE-AC04-94AL85000. This work was performed, in part, at the US Department of Energy, Center for Integrated Nanotechnologies, at Los Alamos National Laboratory (Contract No. DE-AC52-06NA25396) and Sandia National Laboratories (Contract No. DE-AC04-94AL85000).

*joannamm@umich.edu

[1] B. Ferguson and X. Zhang, Nat. Mater. **1**, 26 (2002).
[2] M. Kaminska, Z. Liliental-Weber, E. R. Weber, T. George, J. B. Kortright, F. W. Smith, B.-Y. Tsaur, and A. R. Calawa, Appl. Phys. Lett. **54**, 1881 (1989).
[3] I. S. Gregory, C. Baker, W. R. Tribe, M. J. Evans, H. E. Beere, E. H. Linfield, A. G. Davies, and M. Missous, Appl. Phys. Lett. **83**, 4199 (2003).
[4] A. C. Warren, J. M. Woodall, J. L. Freeouf, D. Grischkowsky, D. T. McInturff, M. R. Melloch, and N. Otsuka, Appl. Phys. Lett. **57**, 1331 (1990).
[5] E. R. Brown, F. W. Smith, and K. A. McIntosh, J. Appl. Phys. **73**, 1480 (1993).
[6] H. Tanoto, J. H. Teng, Q. Y. Wu, M. Sun, Z. N. Chen, S. A. Maier, B. Wang, C. C. Chum, G. Y. Si, A. J. Danner, and S. J. Chua, Nature Photon. **6**, 121 (2012).
[7] X. Lu, D. A. Beaton, R. B. Lewis, T. Tiedje, and M. B. Whitwick, Appl. Phys. Lett. **92**, 192110 (2008).
[8] X. Liu, Y. Sasaki, and J. K. Furdyna, Phys. Rev. B **67**, 205204 (2003).
[9] A. Ohtake, Surf. Sci. Rep. **63**, 295 (2008).
[10] W. Schmidt, Appl. Phys. A: Mater. Sci. Process. **75**, 89 (2002).
[11] J. C. Thomas, N. A. Modine, J. M. Millunchick, and A. Van der Ven, Phys. Rev. B **82**, 165434 (2010).
[12] L. Däweritz and R. Hey, Surf. Sci. **236**, 15 (1990).
[13] H. Nörenberg and N. Koguchi, Surf. Sci. **296**, 199 (1993).
[14] I. Chizhov, G. Lee, R. F. Willis, D. Lubyshev, and D. L. Miller, Phys. Rev. B **56**, 1013 (1997).
[15] M. Masnadi-Shirazi, D. Beaton, R. Lewis, X. Lu, and T. Tiedje, J. Cryst. Growth **338**, 80 (2012).
[16] W. Barvosa-Carter, A. S. Bracker, J. C. Culbertson, B. Z. Nosho, B. V. Shanabrook, L. J. Whitman, H. Kim, N. A. Modine, and E. Kaxiras, Phys. Rev. Lett. **84**, 4649 (2000).
[17] See Supplemental Material at http://link.aps.org/supplemental/10.1103/PhysRevB.87.075320 for more information.
[18] G. Kresse and J. Furthmüller, Phys. Rev. B **54**, 11169 (1996).
[19] M. D. Pashley, Phys. Rev. B **40**, 10481 (1989).
[20] J. M. Sanchez, F. Ducastelle, and D. Gratias, Physica A **128**, 334 (1984).
[21] D. De Fontaine, in *Solid State Physics*, edited by H. Ehrenreich and D. Trunbull (Academic, New York, 1994), p. 33; A. Zunger, in *Statics and Dynamics of Alloy Phase Transformations*, edited by P. E. A. Turchi and A. Gonis, NATO ASI Series, Vol. 319 (Plenum, New York, 1992), p. 361.
[22] J. C. Thomas, J. M. Millunchick, N. A. Modine, and A. Van der Ven, Phys. Rev. B **80**, 125315 (2009).
[23] K. Reuter and M. Scheffler, Phys. Rev. B **65**, 035406 (2001).
[24] O. Romanyuk, V. M. Kaganer, R. Shayduk, B. P. Tinkham, and W. Braun, Phys. Rev. B **77**, 235322 (2008).